Swirl and Tumble Control in Direct Injection Engines using Synthetic Jet Actuators

UNDERGRADUATE HONORS THESIS

Presented in Partial Fulfillment of the Requirements for Graduation with Distinction in the Department of Mechanical and Aerospace Engineering at The Ohio State University

By

John M. Thornton

Undergraduate Program in Mechanical Engineering

The Ohio State University

March 2016

Thesis Examination Committee:

Dr. Vishnu Baba Sundaresan, Advisor

Dr. Manoj Srinivasan

Abstract

In a direct injection engine, fuel injected directly into the combustion chamber mixes with air entering the intake port to form a combustible mixture. Some direct injection engines attempt to optimize this air-fuel mixture near the source of ignition using a movable valve in the intake port which creates swirl and tumble to transport the mixture in a desired direction. However, this valve presents an obstruction to airflow and only provides limited control of the swirl and tumble of air entering the combustion chamber. It was hypothesized that replacing the valve with an array of synthetic jet actuators would remove the physical obstruction in the intake port and allow for greater control of moving air inside the combustion chamber. Synthetic jet actuators contain a chamber, an orifice, and a diaphragm which oscillates at a controlled frequency. The performance of these actuators depends on their dimensions. In this project, the dimensions of the actuator had to be limited to fit on an intake pipe which required them to be smaller than those in other studies. A lumped parameter model was implemented in order to find actuator dimensions which would perform adequately. An actuator was created at these dimensions and tested to determine jet velocities at varying frequencies. Four diaphragms were created to test with the actuator. The diaphragms performed sufficiently producing jet velocities up to 78.05 m/s, however other diaphragms performed insufficiently with maximum jet velocities less than 10 m/s. These findings indicate that a synthetic jet actuator of sufficient size can be created, but more research must be done on creating sufficient diaphragms. The analysis of the small scale synthetic jet actuators used in this study can also find use in many aeronautical applications.

Acknowledgements

I would like to express my sincere gratitude to Dr. Vishnu Baba Sundaresan for providing me with the resources, guidance, and support that allowed me to complete this project. Your advice and expertise has been greatly appreciated and I have enjoyed working with you throughout the project.

I would like to thank Dr. Manoj Srinivasan for attending my defense as a member of my examination committee especially in this busy time of the year. I am grateful for your critiques and the advice that you had to offer.

I would also like to thank Paul Gilmore for his immense knowledge on synthetic jet actuators which he was more than willing to share with me. Your help was greatly appreciated.

I would also like to thank Chad Bivens and Kevin Wolf, the supervisors of the machine shop in the Department of Mechanical and Aerospace Engineering at OSU. You both helped me greatly in machining the synthetic jet actuators for the project.

Lastly, I would like to thank the College of Engineering for providing me with the Undergraduate Research Scholarship to aid in my research. I am honored to be considered worthy of such an award.

Vita

2014 to present…….Undergraduate Research Assistant,
Department of Mechanical and Aerospace
Engineering, The Ohio State University

Fields of Study

Major Field: Mechanical Engineering

Table of Contents

List of Figures

List of Tables

List of Symbols

Symbol	Description
D_O	Orifice Diameter
h	Orifice Height
D_C	Chamber Diameter
H	Chamber Height
R	Inner Radius of Intake Runner
θ	Angle of Section from Array
N	Number of Synthetic Jet Actuators in Array
C_H	Thickness of Clamp on Diaphragm
C_C	Distance Between Edge of Hole and End of Section
Q_D	Flow Rate Produced by Diaphragm
Q_O	Flow Rate Through Orifice
C_{aC}	Chamber Capacitance
V_c	Volume of Chamber
ρ	Density of Working Fluid
a	Speed of Sound
M_{arad}	Acoustic Radiation Inertance
R_{arad}	Acoustic Radiation Resistance
ω	Oscillation Frequency in Radians per Second
M_{al}	Linear Acoustic Inertance
R_{al}	Linear Acoustic Resistance
K_M	Correction Factor for Linear Acoustic Inertance
K_R	Correction Factor for Linear Acoustic Resistance
μ	Dynamic Viscosity

Symbol	Description
R_{anl}	Nonlinear Acoustic Resistance
K_{anl}	Correction Factor for Nonlinear Acoustic Resistance
St	Stoke's Number
ν	Kinematic Viscosity
w	Instantaneous Displacement of Diaphragm
Δ	Peak to Peak Displacement of Diaphragm
r_C	Radius of Chamber
f	Oscillation Frequency in Hertz
u	Instantaneous Velocity of Diaphragm
$Q_{D,max}$	Amplitude of Flow Rate Produced by Diaphragm
u_{peak}	Peak Jet Velocity Produced by Synthetic Jet Actuator
u_{RMS}	Root-Mean Squared Jet Velocity Produced by Synthetic Jet Actuator
$Q_{O,max}$	Peak Flow Rate Through Orifice
$\overline{Q_O}$	Root-Mean Squared Flow Rate Through Orifice
G	Forward Gain in Simulation Block Diagram
$G1$	Loop Gain in Simulation Block Diagram
$Q_{O,sim}$	Simulated Value of Flow Rate Through Orifice

Chapter 1: Introduction

In a direct injection engine, fuel injected directly into the combustion chamber mixes with air entering from the intake port to form a combustible air-fuel mixture. At low or medium engine speeds, creating a stratified air-fuel mixture concentrated close to the spark plug increases the fuel efficiency of the engine [1]. Existing methods for creating this stratified mixture involve using a tumble flap in the intake port [1]. The flap closes at low engine speeds directing incoming air through a smaller inlet. This controls the swirl and tumble of the air in the combustion chamber such that a stratified mixture is created. At high engine speeds, the flap opens allowing a homogeneous mixture to fill the entire chamber. Both of these phenomena are shown in Figure 1.

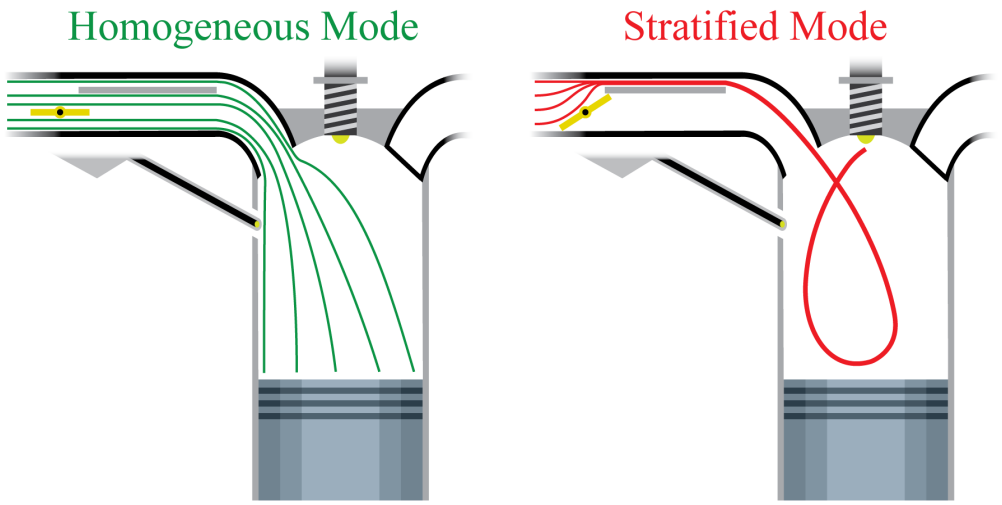

Figure 1. Homogeneous vs. Stratified Mode

While the tumble flap allows for swirl and tumble control, it is not without shortcomings. Even when completely open, the flap provides an obstruction to air flow, and it provides limited control of swirl and tumble of air. An alternative method has been proposed in which the tumble flap is replaced with an array of synthetic jet actuators (SJAs). This project explores the feasibility of implementing this method.

SJAs use acoustic waves to transfer momentum to an ambient fluid [2, 3]. What makes these actuators desirable is that they are zero-net mass-flux actuators meaning they do not require an external supply of fluid to operate [2, 3]. SJAs consist of a piezoelectric diaphragm, chamber, and orifice as shown in Figure 2. The performance of the actuator relies on its dimensions.

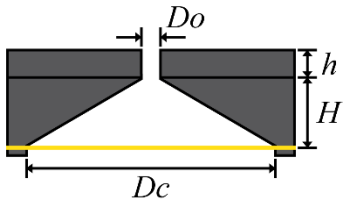

Figure 2. SJA Dimensions

Applying a potential to the diaphragm of the SJA causes it to deform into the chamber. A cyclic variation of applied potential causes fluid to flow through the orifice forming suction and ejection strokes [2]. In order to form a synthetic jet, fluid exiting during the ejection stroke must form a vortex ring [2, 3]. This ring needs to be imparted with enough momentum to overcome suction flow [2, 3].

In order to achieve swirl and tumble control, an array of SJAs can be placed around the intake port to the combustion chamber. Certain actuators can then be activated to direct the incoming air as desired. This concept is illustrated further in Figure 3.

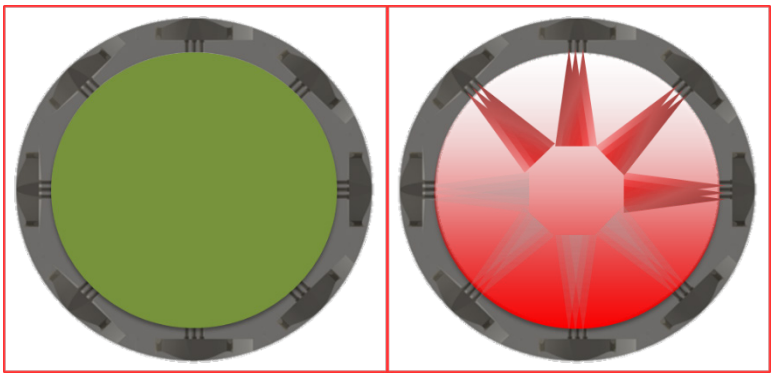

Figure 3. Cross Section of Intake Port with SJA Array

Figure 3 shows a cross section of the intake port with the SJA array in two states. In the left panel, all of the actuators are turned off allowing air to fill the combustion chamber homogeneously. In the right panel, the top actuators are turned on forcing the air downward and creating a stratified mixture. Replacing the tumble flap with an array of SJAs theoretically offers two advantages. The first advantage is that it removes the obstruction caused by the tumble flap. The second advantage is that a SJA array would provide more control by allowing air to be directed in any direction.

1.1 Focus of Thesis

The purpose of this project was to design and characterize a SJA at a small enough scale to be implemented in an array for swirl and tumble control in a direct injection engine. The

project involved designing, fabricating, and testing a SJA of an appropriate size. Since the performance of a SJA is influenced by its dimensions, a lumped parameter model of a SJA was implemented to aid in the determination of appropriate actuator dimensions. After determining the appropriate dimensions, a SJA was fabricated and tested to ensure that it could produce adequate jet velocities.

1.2 Significance of Research

Developing vehicles with increased fuel efficiency while not sacrificing power is a major objective in the automobile industry [1]. In-cylinder air motion has a significant effect on both of these and should be optimized to produce more fuel efficient vehicles [4]. Research suggests that, by eliminating in-cylinder cyclic variations, a 10% improvement in engine power output could be obtained for the same fuel consumption [5]. In-cylinder cyclic variations are affected by intake flow cyclic variations [4]. Therefore, it is possible that SJAs could be used to eliminate intake flow cyclic variations which would lead to better fuel efficiency.

SJAs have many other applications as well. For example, they have proved useful as mixing devices and have been researched for use in boundary layer manipulation [6, 7]. While research on SJAs exists, there is little research on smaller scale SJAs such as those implemented in this project. Small scale SJAs could prove useful in many flow control applications where size is a constraint.

1.3 Overview of Thesis

This thesis has 7 chapters. Chapter 2 discusses the determination of the dimensions for the SJA. This chapter includes discussion about the design constraints due to the size of the

intake pipe and the lumped parameter model used in selecting dimensions. Chapter 3 discusses the fabrication of the SJA. This chapter includes the fabrication of the actuator itself as well as the process for creating diaphragms. Chapter 4 discusses the experimental characterization of the SJA to find jet velocities. Chapter 5 lays out the results from experimental characterization and includes an analysis and discussion of the results. Chapter 7 concludes the thesis by summarizing the contributions of this project and proposing future research.

Chapter 2: Determination of Synthetic Jet Actuator Dimensions

In order to design a SJA array, the dimensions of the SJAs in the array needed to be specified. These dimensions significantly affect the performance of the SJA and were constrained by the size of the intake port. Therefore, specifying the dimensions required extensive analysis. An initial design was first created and analyzed so that the size constraints due to the intake port could be determined. Optimal geometric ratios obtained from literature were then implemented to ensure adequate SJA performance. A lumped element model of SJAs was then implemented using MATLAB and Simulink to obtain simulated velocity responses of SJAs at the specified dimensions.

2.1 Initial Design of SJA Array

Designing the SJA array involved many geometric constraints due to the size of the intake port. An initial design of the array was created so these constraints could be understood clearly. This design is shown fully in Figure 4 and a cross section is shown in Figure 5

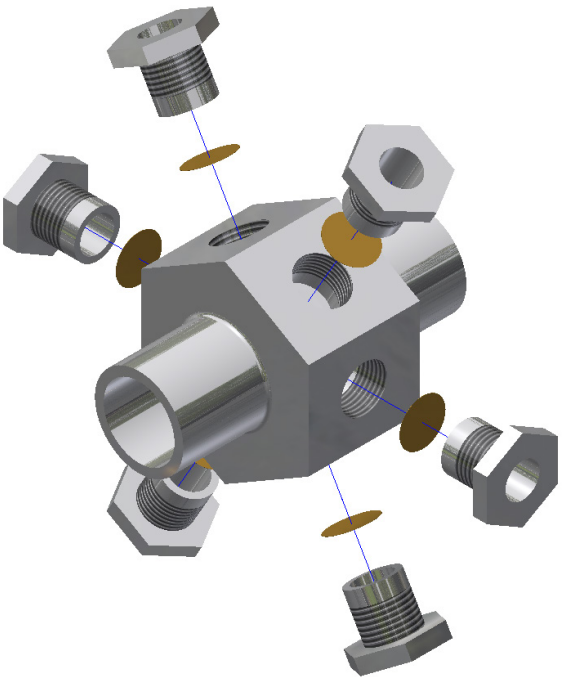

Figure 4. Initial Design of SJA Array

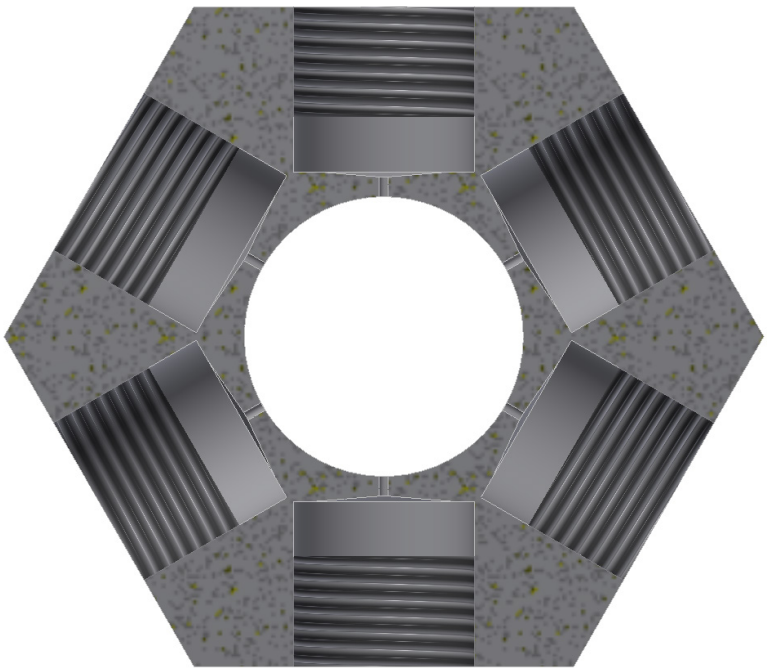

Figure 5. Cross Section of SJA Array Initial Design

In this design, the diaphragms are clamped to the chamber using hollow bolts. The actuators have conical chambers instead of the more common cylindrical ones. Conical chambers were chosen based on research conducted by Paul Gilmore suggesting that they produce higher jet velocities.

2.2 Geometric Model

Using this design, a geometric model was created to convert the physical constraints into mathematical ones. The geometric model cuts the design into sections based on the number of actuators in the array. This model is shown in Figure 6.

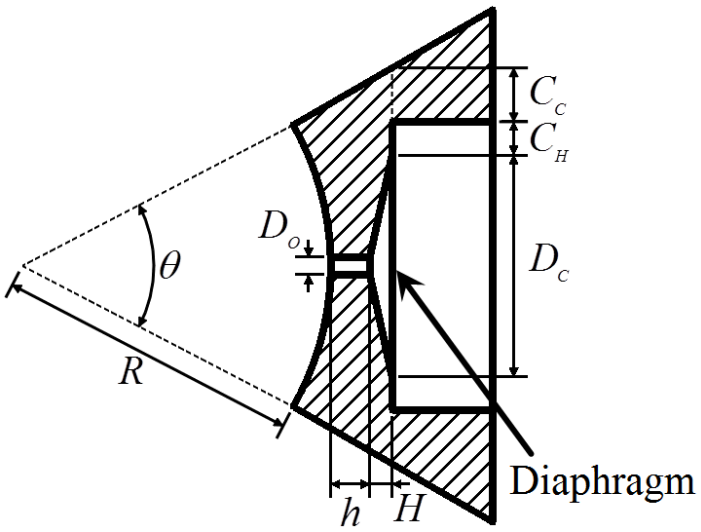

Figure 6. Geometric Model of SJA Array

In the geometric model, R represents the radius of the intake port and has been set at 0.5 inches as it is a nominal value and close to values found in literature [4, 8]. θ represents the section angle and depends on the number of actuators in the array. It is given by

$$\theta = \frac{2\pi}{N} \tag{1}$$

where N is the number of actuators in the array. This was initially chosen to be 8, however having 8 actuators would limit the size of the chamber diameter, and thus, the amount of lead zirconate titanate (PZT), the piezoceramic material used to actuate the diaphragm. Therefore, N was changed to 6 so an adequate amount of PZT could be used.

C_H represents the thickness of the clamp on the diaphragm and has been chosen to be 2 mm. C_H should be long enough so the diaphragm can be clamped securely. C_C represents the distance between the edge of the hole and the end of the section and has been chosen to be 0.5 mm. C_C needs to be present so the hole does not interfere with holes of adjoining sections. D_C, H, D_O, and h represent the chamber diameter, chamber height, orifice diameter, and orifice height of the SJA. The geometric model reduces D_C to a function of h and H given by

$$D_C = 2\left[-C_C - C_H + \left(R + h + H\right)\tan\left(\frac{\theta}{2}\right)\right] \tag{2}$$

h and H can both be reduced to functions of D_O using optimal geometric ratios found from literature. SJAs satisfying these ratios achieve the highest peak jet velocities as shown by Gomes et. al. [9]. The ratios are given by $H / D_O = 0.6$ and $h / D_O = 2.1$.

2.4 Lumped Element Model

After reducing the actuator dimensions to a function of D_O, implementation of a lumped element model for SJAs allowed the determination of theoretical jet velocities [10]. Figure 7 shows an equivalent circuit representation of the model.

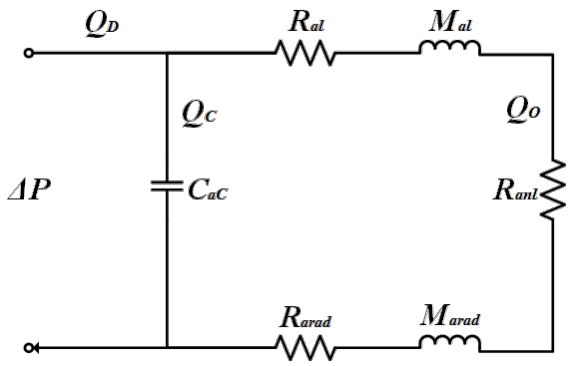

Figure 7. Circuit Representation of Lumped Element Model

In the model, Q_D represents the flow rate produced by the diaphragm, and Q_O represents the flow through the orifice. The model decouples the motion of the diaphragm from the fluid flow in the cavity so the fluid mechanics can be better analyzed [10]. The model also assumes that the largest dimension of the actuator is much smaller than the acoustic wavelength which means the validity of the model degrades at high frequencies.

C_{aC} represents the acoustic compliance of the cavity and can be obtained assuming that the fluid is isentropic and an ideal gas

$$C_{aC} = \frac{V_c}{\rho a^2} \tag{3}$$

where V_c is the volume of the cavity, ρ is the density of the fluid, and a is the isentropic speed of sound [10]. M_{arad} and R_{arad} represent the acoustic mass and resistance due to radiation. They are obtained by modeling the actuator as a piston in a semi-infinite baffle

$$R_{arad} = 0.159\frac{\rho\omega^2}{a} \tag{4}$$

$$M_{arad} = \frac{16\rho}{3\pi^2 D_O} \tag{5}$$

where D_O is the orifice diameter and ω is the operating frequency [10]. M_{al} and R_{al} can be obtained by modeling the flow through the orifice as steady laminar flow and adding correction factors K_M and K_R

$$M_{al} = K_M \frac{16\rho h}{3\pi D_O^2} \tag{6}$$

$$R_{al} = K_R \frac{128\mu h}{\pi D_O^4} \tag{7}$$

where h is the length of the orifice and μ is the dynamic viscosity of the fluid [10]. R_{anl} takes into account the minor losses associated with entrance and exit effects at the orifice [10]. Its dependence on Q_O makes it a nonlinear term

$$R_{anl} = R'_{anl} Q_O = K_{anl} \frac{8\rho Q_O}{\pi^2 D_O^4} \tag{8}$$

where K_{anl} is a loss coefficient dependent on the velocity profile [10]. K_R, K_M, and K_{anl} are all functions of the Stokes number associated with the flow which is given by

$$St = \sqrt{\frac{\omega D_O^2}{\nu}} \tag{9}$$

where ν is the kinematic viscosity of the fluid. The governing differential equation for the model is given by

$$C_{aC}\left(M_{al} + M_{arad}\right)\ddot{Q}_O + C_{aC}\left(R_{al} + R_{arad} + 2R_{anl}\right)\dot{Q}_O + Q_O = Q_D \tag{10}$$

Q_D can then be calculated using the theory of plates and shells [11]. This is done by first calculating the instantaneous displacement of the diaphragm assuming it is a circular plate loaded at the center

$$w(r,t) = \frac{\Delta}{2}\left[1 - \frac{r^2}{r_C^2} + \frac{2r^2}{r_C^2}\ln\left(\frac{r}{r_C}\right)\right]\sin(\omega t) \tag{11}$$

where Δ is the peak to peak displacement of the diaphragm and r_C is the radius of the chamber [11]. In this project, Δ is assumed to be a constant value of 5 microns. The instantaneous velocity can then be found by taking the derivative with respect to time

$$u(r,t) = \pi \Delta f\left[1 - \frac{r^2}{r_C^2} + \frac{2r^2}{r_C^2}\ln\left(\frac{r}{r_C}\right)\right]\cos(\omega t) \tag{12}$$

where f is the oscillation frequency in hertz [11]. This can then be integrated over the entire diaphragm

$$Q_D(t) = \frac{\pi^2}{16}\Delta f D_C^2 \cos(\omega t) \tag{13}$$

$$Q_{D,max} = \frac{\pi^2}{16}\Delta f D_C^2 \tag{14}$$

where D_C is the chamber diameter.

2.5 Implementation Using MATLAB and Simulink

Frequency responses can be simulated showing the peak and root mean squared velocities of the actuator using the model with MATLAB and Simulink. Peak velocity and RMS velocity are given by

$$u_{peak} = \frac{4Q_{O,max}}{\pi D_O^2} \tag{15}$$

$$u_{rms} = \frac{4\overline{Q_O}}{\pi D_O^2} \tag{16}$$

where $Q_{O,max}$ is the maximum value of Q_O at steady state, and $\overline{Q_O}$ is the mean value of Q_O at steady state. The Simulink block diagram is shown in Figure 8.

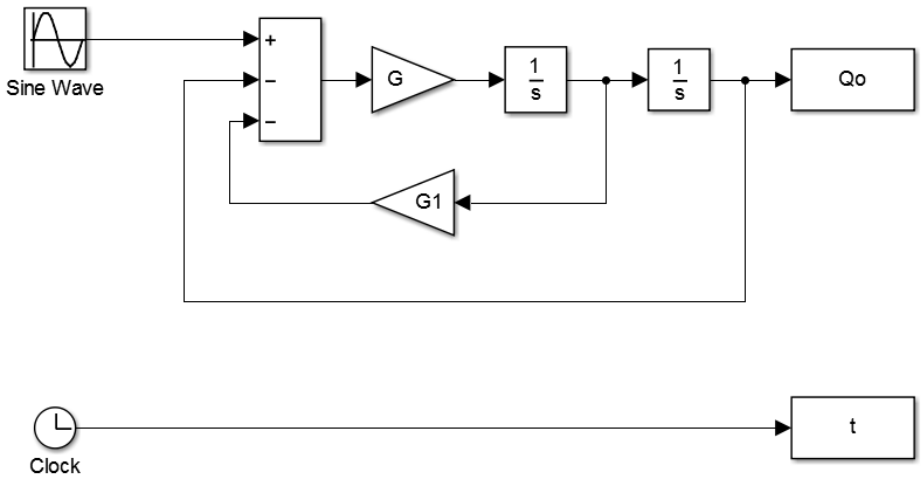

Figure 8. Lumped Element Model Block Diagram

In the diagram, the frequency of sine wave input is set to the oscillation frequency, ω, while the amplitude is set to $Q_{D,max}$. The two gains of the system are given by

$$G = \frac{1}{C_{aC}\left(M_{al} + M_{arad}\right)} \tag{17}$$

$$G1 = 2C_{aC}\left(R'_{anl} Q_{O,sim}\right) \tag{18}$$

The model is iterated over 10 cycles to calculate the steady-state jet velocity. $Q_{O,sim}$ is set to either the maximum value of Q_O or its root-mean squared value after each iteration depending on the response being simulated. To create a frequency response, this process is repeated throughout a range of frequencies. Figures 9 and 10 demonstrate the effect that the number of iterations has on the steady state time and frequency responses.

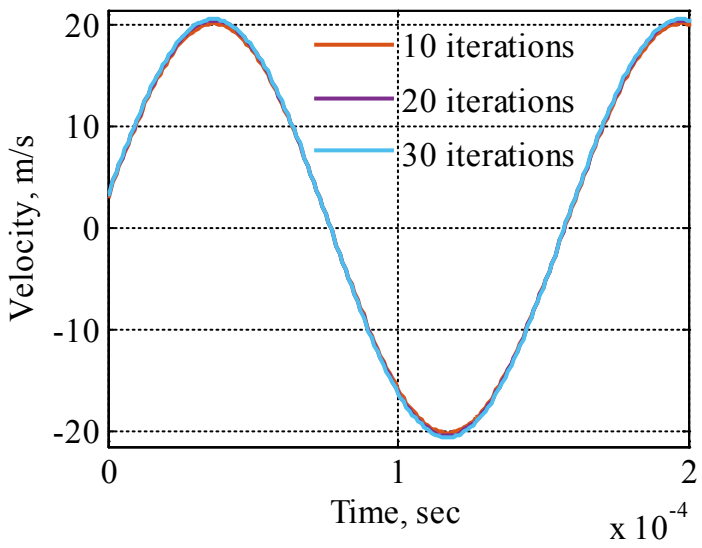

Figure 9. Convergence of Velocity at Steady State

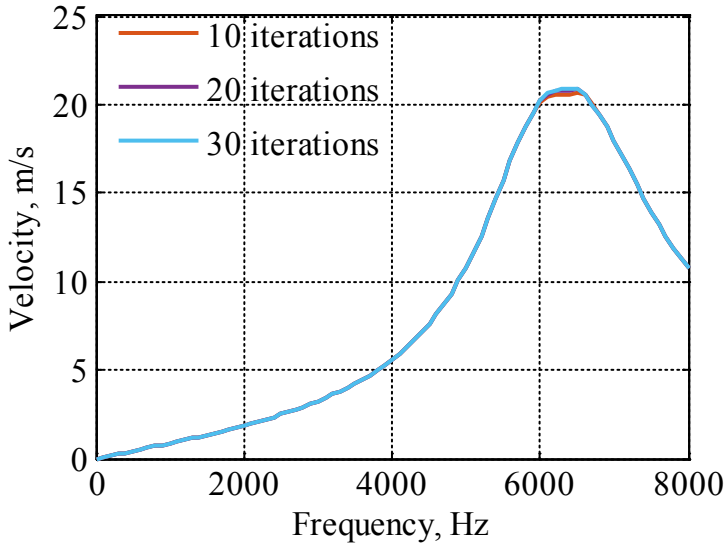

Figure 10. Convergence of Frequency Response

The system shown in Figures 9 and 10 is simulated using the SJA dimensions selected in Section 2.6. The steady state response plotted in Figure 10 is excited at the natural frequency, 6200 Hz, which is where convergence problems are most significant. However, even at this frequency, 10 iterations is enough for convergence to occur.

To aid in the determination of SJA dimensions, frequency responses were simulated over a range of orifice diameters. The results can be seen in Figure 11.

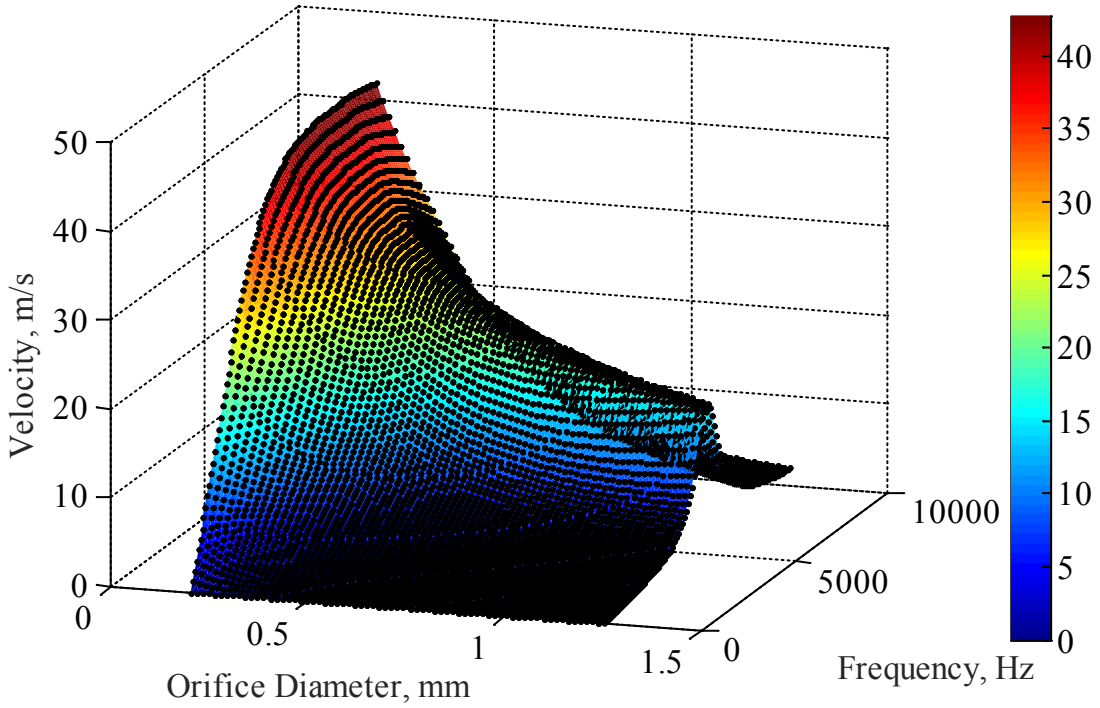

Figure 11. Simulated Peak Jet Velocities at Varying Frequencies and Orifice Diameters

The peak velocity increases as D_O decreases, but so does D_C. If D_C is too small, an adequate amount of PZT cannot be used to actuate the diaphragm. Also it is important that D_O be large enough so that the actuator can be actually be machined.

2.6 Selected Dimensions for SJA

Taking all of these constraints into account, D_O was set as 0.84 mm or 0.033 inches. It was thought that, at this value, D_C would be large enough for an adequate amount of PZT to be used. Also, 0.033 inches is a standard drill size (#66). Specifying D_O set all other dimensions of the actuator as well. They are all shown in Table 1.

Table 1. Dimensions of SJA for Array

D_O	0.84 mm
h	1.76 mm
D_C	12.28 mm
H	0.50 mm
V_C	21.30 mm^3

The frequency response for these values was then simulated to find peak velocities and is shown in Figure 12. The simulated RMS velocities are shown in Figure 13.

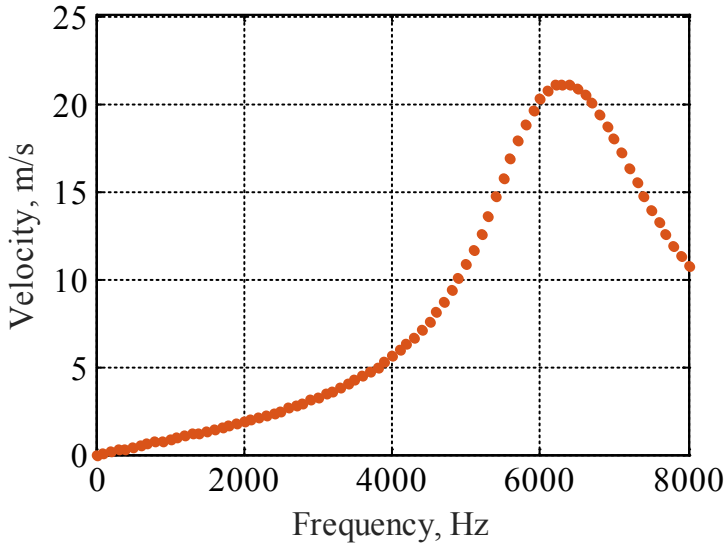

Figure 12. Simulated Peak Velocities at Various Frequencies with Do = 0.84 mm

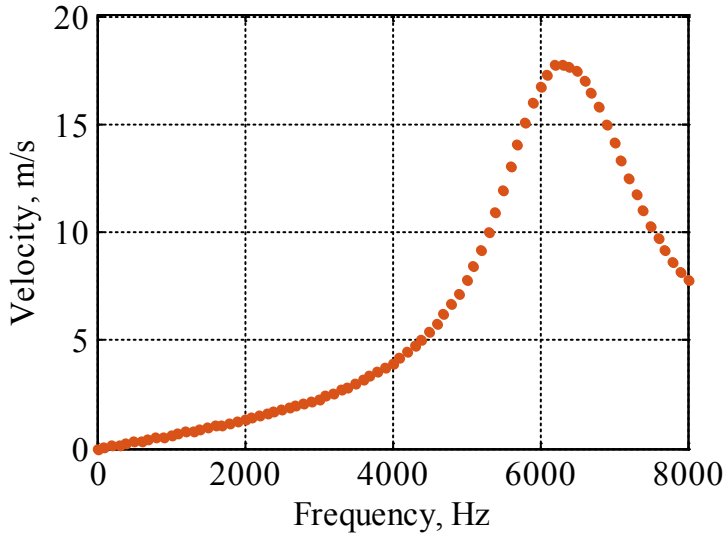

Figure 13. Simulated RMS Velocities at Various Frequencies with Do = 0.84 mm

For the peak velocity simulation, the natural frequency occurs at 6200 Hz with a peak velocity of 21.12 m/s. The natural frequency from the RMS velocity simulation is 6300 Hz and the maximum RMS velocity is 17.77 m/s. The acoustic wavelength at this frequency is 55 mm, and the chamber diameter is the largest dimension at 12.3 mm. Therefore, the acoustic wavelength is 4.5 times greater than the chamber diameter, and the model is probably valid.

2.7 Chapter Summary

Models were used to aid in the selection of appropriate SJA dimensions for the SJA array. First, an initial model of the array itself was created and analyzed to determine the size constraints due to the intake port. Secondly, optimal geometric ratios were implemented to augment the performance of the SJA. A lumped element model was then implemented using MATLAB and Simulink to simulate jet velocities at various frequencies for selected dimensions. The dimensions of the SJA were then specified and can be found in Table 1. Peak jet velocities and RMS velocities were then simulated at the specified dimensions over various frequencies. The maximum simulated peak jet velocity was 21.12 m/s and occurred at 6200 Hz while the maximum simulated RMS velocity was 17.77 m/s and occurred at 6300 Hz.

Chapter 3: Synthetic Jet Actuator Fabrication and Characterization

In the previous chapter, the dimensions of the SJA were specified and theoretical peak and RMS jet velocities were simulated over a range of frequencies. This chapter discusses the fabrication of a SJA at the specified dimensions as well as its experimental characterization based on jet velocities. Much of this chapter focuses on diaphragm fabrication as this process causes a high degree of variability.

3.1 SJA Design and Fabrication

A SJA of the selected dimensions was designed using Solidworks and Autodesk Inventor. Engineering drawings of the SJA can be found in Appendix C. The SJA was machined from 6061 aluminum to the specified dimensions and is shown fully assembled in Figure 14.

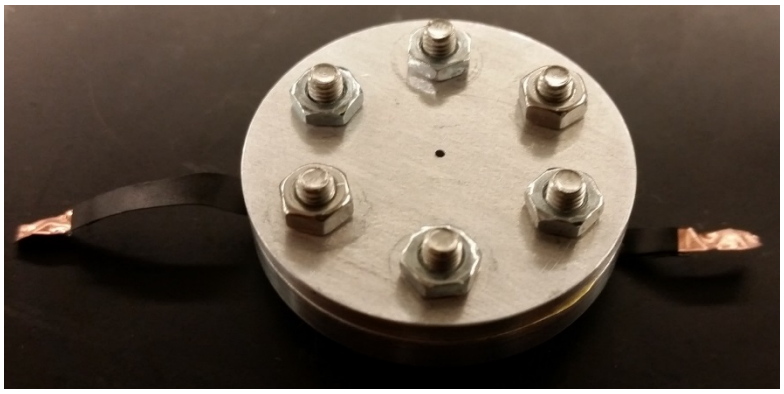

Figure 14. SJA at Array Dimensions

Screws and nuts are necessary to hold the diaphragm in place. The diaphragm is restrained between the chamber cavity of the SJA and an aluminum cover. A PZT disk is attached and centered on the underside of the diaphragm to provide the driving force. An exploded view of the SJA design can be seen in Figure 15.

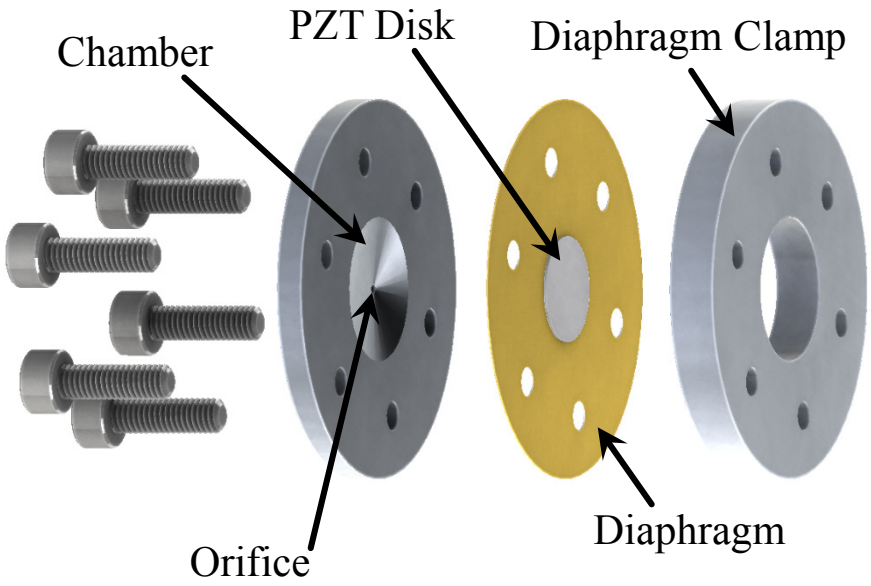

Figure 15. Exploded View of SJA Design

3.2 Diaphragm Fabrication

Diaphragms are cut from 0.005 inch thick brass shim stock and actuated with a 0.0108 inch thick PZT-5H ceramic disk adhered using super glue. The PZT disk is cut from a sheet using a diamond scribe. Copper tape adhered to the PZT disk provides leads to which an input potential can be applied. The diaphragm is shown in Figure 16.

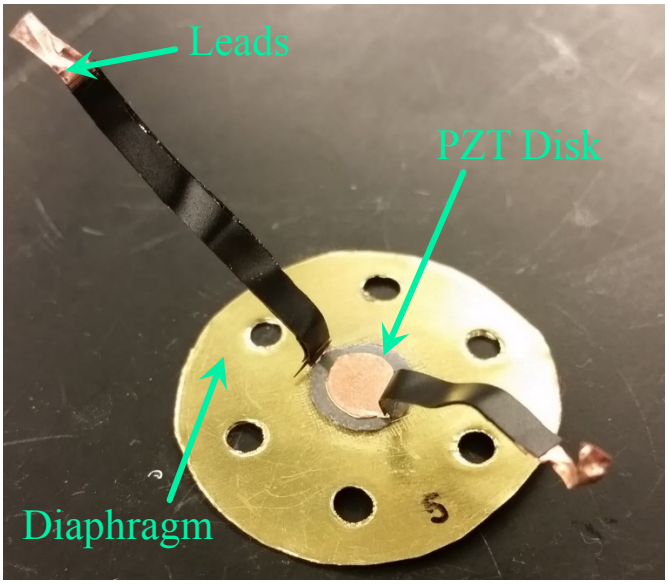

Figure 16. SJA Diaphragm

Cutting out PZT disks presented a major source of variability in the diaphragm fabrication process. Initially diaphragms were cut manually, but due to the brittle nature of PZT, making controlled cuts was nearly impossible. Therefore, a motor guide assembly was implemented to alleviate this problem. The assembly setup is shown in Figure 17.

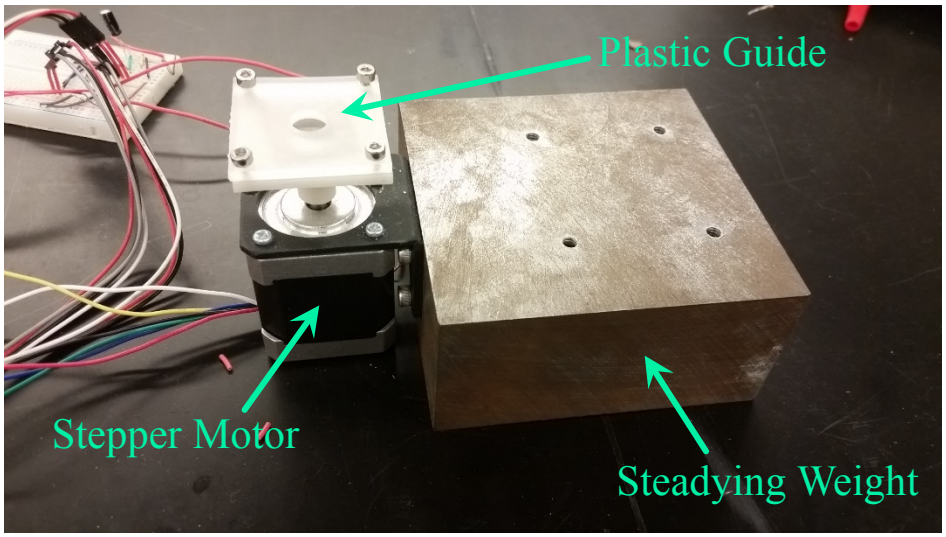

Figure 17. Motor Guide Assembly Setup

The PZT sheet is clamped under a plastic guide. The diameter of the guide hole is 9.90 mm. The motor rotates slowly allowing the diamond scribe to move along the guide as shown in Figure 18.

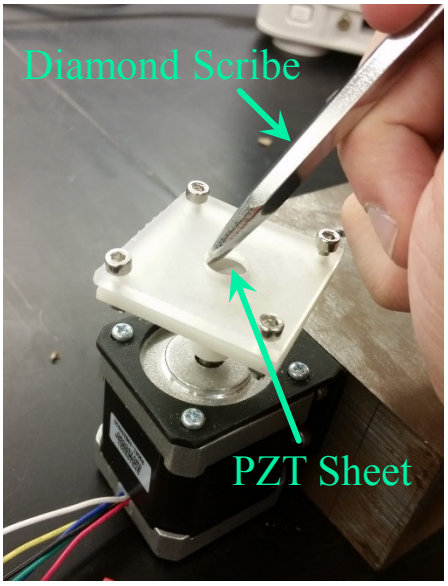

Figure 18. Motor Guide Assembly in Use

Even with the motor guide, uncertainty with the diaphragms still exists due to other steps in the fabrication process including the bonding of the PZT disk to the brass shim. In an effort to quantify this uncertainty, the weight of super glue used when adhering the PZT disk to the brass diaphragm was measured for each diaphragm except the first one made. An apparatus was also developed to apply and measure a bond force to the diaphragm after applying the super glue. However, it was found that the device put indents into the diaphragm which negatively affected their performance. Four diaphragms were fabricated and tested. The properties of each diaphragm are given in Table 2. Note that the PZT disk diameter on diaphragm 1 is smaller than the others. This is because the tip of the diamond scribe was not flush with the motor guide during cutting.

Table 2. Diaphragm Properties

#	**Diameter of PZT Disk (mm)**	**Weight of Glue (mg)**
1	9.0	N/A
2	9.9	10.4
3	9.8	7.1
4	9.9	9.7

3.3 Setup for Measuring Jet Velocity

A constant temperature anemometry (CTA) probe, suspended over the orifice of the SJA, measured jet velocity during characterization. A plastic stand assembly holds the probe directly

over the orifice at a distance of 0.05 inches from the orifice exit. This assembly can be seen in Figure 19 and a close-up of the SJA can be seen in Figure 20.

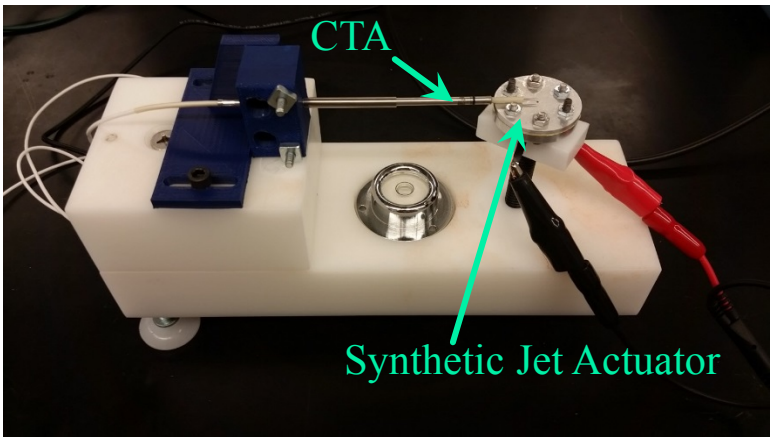

Figure 19. Setup for Holding SJA

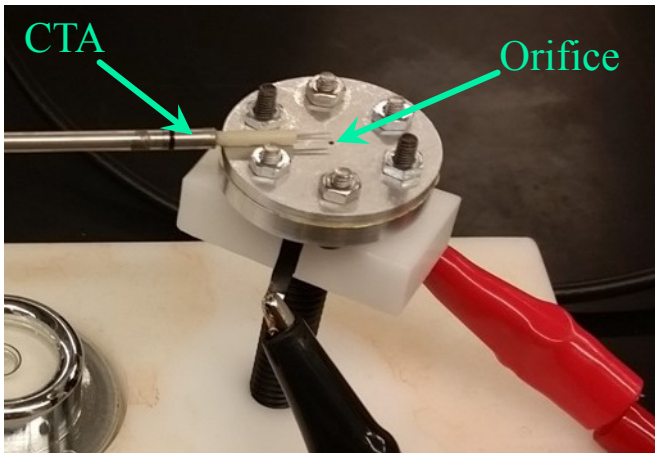

Figure 20. Close-Up of CTA Probe over Orifice

A sinusoidal input potential was applied to the diaphragm using a signal generator along with an amplifier. Velocity data was recorded using an oscilloscope and transferred to a computer for post processing in MATLAB. The amplitude of the sinusoidal input produced by the signal generator was set at 3.5V and the frequency was set to the oscillation frequency of the diaphragm. The amplifier adds a gain of 20 to the input signal. The entire setup is shown in Figure 21.

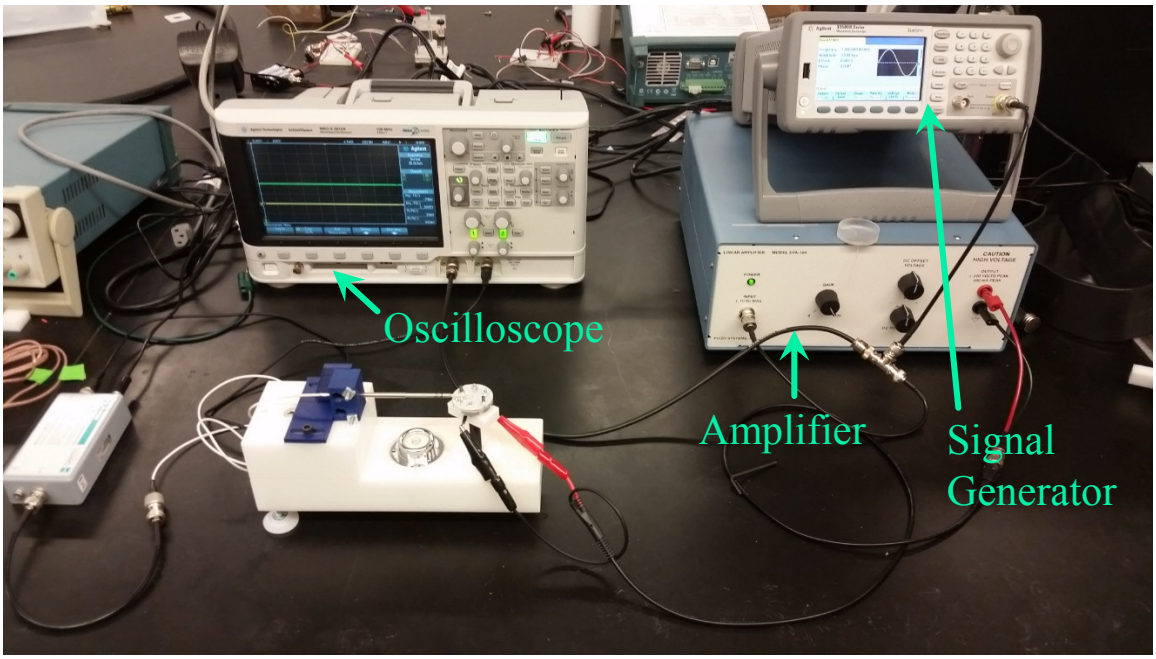

Figure 21. Setup for Measuring Jet Velocity

3.4 Chapter Summary

Because the performance of a SJA relies heavily on its dimensions, it was important to experimentally characterize an actuator at the selected dimensions from Chapter 2 based on jet velocities. A SJA was designed with the selected dimensions and machined. There was much

variability inherent to the diaphragm fabrication process which made it necessary to test on multiple diaphragms. Therefore, four diaphragms were created to test with, and their properties are listed in Table 2. During tests a sinusoidal input was applied, and the jet velocity was measured using a CTA probe. The frequency response of the actuator was acquired by measuring the velocity over a range of frequencies. At each frequency, the peak and RMS velocity was extracted from the steady state portion of the measured velocity data. A frequency response was plotted for each of the four diaphragms and is discussed in Chapter 4.

Chapter 4: Results and Discussion

In Chapter 2, simulated peak and RMS jet velocities for a SJA at specified dimensions were obtained over a range of frequencies and briefly discussed. In Chapter 3, a SJA satisfying these specific dimensions was created and the procedures for characterizing the SJA for peak and RMS jet velocities were outlined. In this chapter, the results from these tests will be discussed and analyzed in comparison with each other and the results from simulation.

4.1 Experimental Peak Velocity over Varying Frequencies

The peak jet velocity of the SJA was obtained for each diaphragm over a range of frequencies. This frequency response is shown in Figure 22. A statistical analysis of the natural frequencies and their corresponding peak velocities is reported in Tables 3 and 4. Note that there are two resonant frequencies present in the experimental results. The higher resonant frequency is due to diaphragm resonance while the lower resonant frequency is the acoustic resonant frequency or the Helmholtz frequency [9].

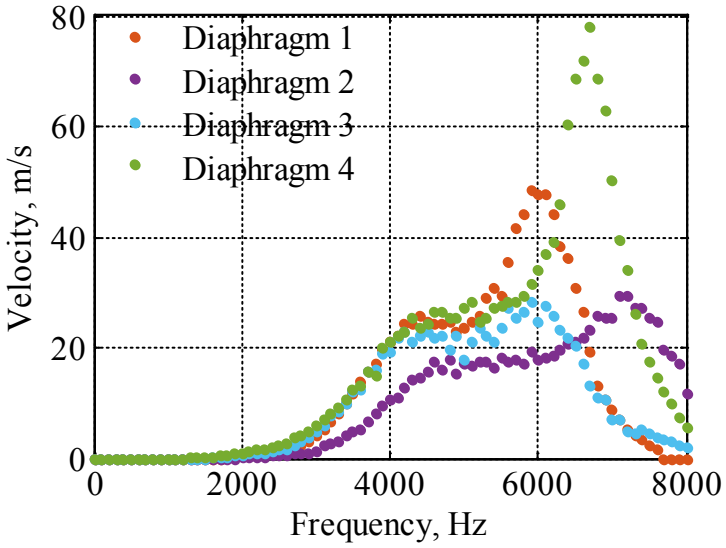

Figure 22. SJA Peak Velocities over a Range of Frequencies

Table 3. Resonant Frequency and Peak Velocity Statistics at Acoustic Resonance

Diaphragm #	Frequency (Hz)	Peak Velocity (m/s)	% Difference (Frequency)	% Difference (Velocity)
1	4400	25.93	3.83	11.35
2	4800	18.01	4.92	22.66
3	4500	22.71	1.64	2.48
4	4600	26.50	0.55	13.79
Mean	4575	23.29	2.73	12.57
Standard Deviation	171	3.89		

Table 4. Resonant Frequency and Peak Velocity Statistics at Diaphragm Resonance

Diaphragm #	Frequency (Hz)	Peak Velocity (m/s)	% Difference (Frequency)	% Difference (Velocity)
1	5900	48.49	8.2	5.2
2	7200	29.50	12.1	36.0
3	5900	28.27	8.2	38.6
4	6700	78.05	4.3	69.4
Mean	6425	46.08	8.2	37.3
Standard Deviation	640	23.24		

From Tables 3 and 4, it can be seen that diaphragm 4 had the largest resonant peak velocity at 78.05 m/s. This value doubles that from diaphragms 2 and 3. Diaphragms 2 and 3 achieve similar maximum peak velocities, but their resonant frequencies are over 1000 Hz apart. In general, the diaphragm resonant frequencies and peak velocities vary significantly with each run, and the acoustic resonance frequencies and velocities are more consistent. This is to be expected as the diaphragm is different in each test, however it gives insight into the degree of variability present in the diaphragm fabrication process. After examining each of the 4 diaphragms, it was the noticed that those which performed better seemed to exhibit a snap through motion when a small amount of force was applied to the center of the diaphragm. This may explain the reason for the success of these diaphragms. While more evidence is needed to determine whether this is the case, inducing such a snap through motion may be useful in creating better performing diaphragms for SJAs.

4.2 Experimental RMS Velocity over Varying Frequencies

A frequency response was also obtained for the RMS velocities and is shown in Figure 23. Tables 5 and 6 present a statistical analysis of the RMS natural frequencies.

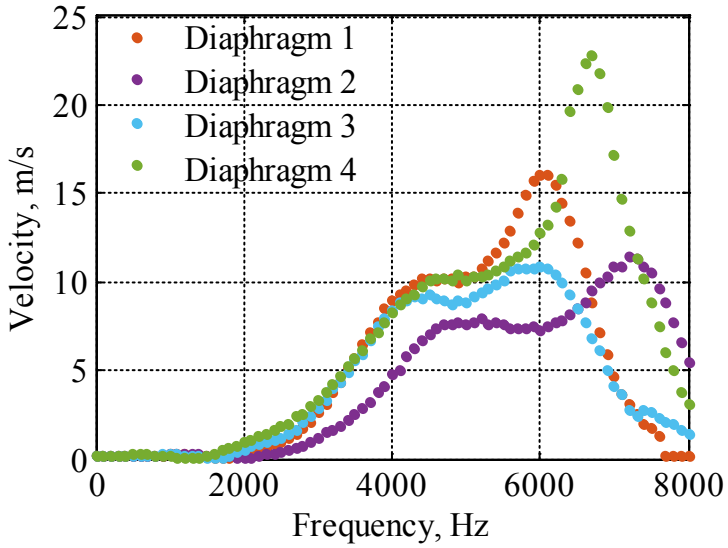

Figure 23. SJA RMS Velocities over a Range of Frequencies

Table 5. Resonant Frequency and RMS Velocity Statistics at Acoustic Resonance

Diaphragm #	Frequency (Hz)	RMS Velocity (m/s)	% Difference (Frequency)	% Difference (Velocity)
1	4400	10.21	6.4	8.6
2	5200	7.89	10.6	16.1
3	4500	9.30	4.3	1.1
4	4700	10.20	0	8.5
Mean	4700	9.40	5.3	8.6
Standard Deviation	356	1.09		

Table 6. Resonant Frequency and RMS Velocity Statistics at Diaphragm Resonance

Diaphragm #	Frequency (Hz)	RMS Velocity (m/s)	% Difference (Frequency)	% Difference (Velocity)
1	6000	16.02	7.3	5.0
2	7200	11.39	11.2	25.4
3	6000	10.84	7.3	29.0
4	6700	22.79	3.5	49.3
Mean	6475	15.26	7.3	27.2
Standard Deviation	585	5.53		

The frequency response for the RMS velocities looks very similar in shape to the peak velocity frequency response, but the velocities are lower. The maximum RMS velocity again belongs to diaphragm 4 at 22.79 m/s. The location of acoustic resonance frequency does appear to be slightly less consistent, however the acoustic resonant RMS velocities are still significantly

more consistent than the diaphragm resonant frequency velocities. In order to increase the consistency at the diaphragm resonant frequency, the diaphragm fabrication process should be examined thoroughly.

4.3 Comparisons between Simulations and Experiments

The experimental frequency responses can also be compared with the simulated frequency responses. Table 7 shows a statistical analysis of the simulation values compared to the mean values from the experiments.

Table 7. Comparison of Simulation and Mean Experiment Values at Acoustic Resonance

	Peak Response		**RMS Response**	
	Frequency (Hz)	**Velocity (m/s)**	**Frequency (Hz)**	**Velocity (m/s)**
From Simulation	6200	21.12	6300	17.77
Mean from Experiments	4575	23.29	4700	9.4
% Difference	35.5	9.3	34.0	89.0

In comparing the simulation to the experimental mean values, the simulation appears to be decently accurate at predicting peak velocities at the Helmholtz frequency. However, it does not seem to be accurate at predicting the Helmholtz frequency itself. Interestingly, the Helmholtz frequency predicted from the simulation was much closer to the diaphragm natural frequency, but this is a coincidence. It is not appropriate to compare the diaphragm resonance values to those from the simulation. The simulation does not

predict a diaphragm resonance because the diaphragm is decoupled from the lumped element model that was used.

4.4 Chapter Summary

In this chapter, the peak and RMS jet velocity responses obtained from experiments were examined. Velocity results were promising with peak velocities reaching 78.05 m/s. However, performance of the actuator was heavily dependent on the diaphragm. Each diaphragm performed differently with the diaphragm natural frequency and resonant jet velocities varying, while the acoustic natural frequency was more consistent between diaphragms. The diaphragm resonance frequency was important in producing high jet velocities, usually dominating the acoustic resonance.

The lumped element model used with MATLAB and Simulink in Chapter 2 was compared to the experimentally measured responses. The model was inaccurate in identifying the Helmholtz frequencies, over reporting the value by 34%. Even with this error, the model did seem to accurately predict the peak velocity at the Helmoltz frequency. That being said, there has not been enough analysis to confirm or deny the validity of the lumped parameter model.

Chapter 5: Conclusions

The use of synthetic jet actuators for the control of swirl and tumble of air in direct injection engines is suggested as an alternative to the existing method of using a tumble flap in the intake port. While the tumble flap is used to direct the air to the spark plug, thus creating a stratified mixture, it presents an obstruction to airflow even when fully open. Replacing the tumble flap with an array of SJAs would eliminate this obstruction and could theoretically provide other benefits including increased swirl and tumble control.

A SJA of ideal size to fit in an array of actuators around a 1 inch diameter intake port was designed, fabricated, and characterized by its jet velocity. Extensive use of modeling during the design process allowed an optimal SJA to be created. Experimental characterization of the SJA showed promising results indicating that the small scale SJA could be implemented in a SJA array for swirl and tumble control with jet velocities reaching 78.05 m/s. This value can be compared to average intake runner air velocities, which reach around 6 m/s [4]. Therefore, the SJA should be capable of affecting in-cylinder air motion.

Diaphragm fabrication introduced a large amount of variability as each diaphragm performed differently. This process should be analyzed to see if more improvements can be made. While examining each of the diaphragms, it was noticed that the better performing actuators tended to have a snap through motion when the center of the diaphragm was pressed. It is possible that this snap through motion was responsible for the success of these diaphragms and may be implemented in the optimization of future diaphragms.

5.1 Contributions to the field

A major contribution of this thesis is the analysis of a synthetic jet actuator that is of comparable size to be added to an intake runner port. While there is much research on larger SJAs, not much has been done on SJAs at this scale. The primary purpose of this thesis was to produce an actuator that was suitable for swirl and tumble control applications, but an actuator at this size could be useful for other flow applications in which size is a constraint. This work also added to knowledge on the lumped element model used for simulating the frequency response. An in depth analysis of the model was included and a comparison between the model and the experimental results provided evidence as to the accuracy of the model for SJAs at this size.

5.2 Future Work

Future work should involve the creation of a SJA array and the testing of its ability to control the swirl and tumble of air in a direct injection engine. Other work can include optimization of SJA diaphragms which could possibly utilize the snap through motion that was characteristic of the diaphragms which performed well. Lastly, future work could also include creating and understanding the dynamics of synthetic jet actuators on an even smaller scale.

Bibliography

[1] Audi AG. (2001). *IAA 2001: FSI - The Direct-Injection Petrol Engine* [Online]. Available: http://www.audiworld.com/news/01/iaa/fsi/content.shtml

[2] A. Glezer and M. Amitay, "Synthetic Jets," *ARFM*, vol. 34, pp. 503-529, 2002.

[3] R. Holman *et al*., "Formation Criterion for Synthetic Jets," *AIAA*, vol. 43, no. 10, pp. 2110-2116, Oct. 2005.

[4] T. Justham *et al*., "Simultaneous Study of Intake and In-Cylinder IC Engine Flow Fields to Provide an Insight into Intake Induced Cyclic Variations," *J. Phys.: Conf. Series*, vol. 45, pp. 146-153, 2006.

[5] N. Ozdor, *et al*., "Cyclic Variability in Spark Ignition Engines – A Literature Survey," SAE Tech. Paper, no. 940987, 1994.

[6] M. Al-Atabi, "Experimental Investigation of the Use of Synthetic Jets for Mixing in Vessels," *J. Fluids Eng.*, vol. 133, Sep. 2011.

[7] M. Amitay *et al*., "Aerodynamic flow control over an unconventional airfoil using synthetic jet actuators," *AIAA*, vol. 39, no. 3, pp. 361-370, 2001.

[8] L. Cui *et al*., "Full-Parameter Approach for the Intake Port Design of a Four-Valve Direct-Injection Gasoline Engine," *J. Eng. Gas Turbines Power*, vol. 137, no. 9, pp. 91502, Sep. 2015.

[9] L. D. Gomes, *et al*., "Towards a practical piezoceramic diaphragm based synthetic jet actuator for high subsonic applications – effect of chamber and orifice depth on actuator peak velocity," in *3rd AIAA Flow Control Conf.*, San Francisco, 2006, pp. 267-283.

[10] H. Tang and S. Zhong, "Lumped element modeling of synthetic jet actuators," *Aerospace Science and Technology*, vol. 13, no. 6, pp. 331-339, Sep. 2009.

[11] S. Timoshenko and S. Woinowsky-Krieger, "Large Deflections of Plates" in *Theory of Plates and Shells*, 2nd ed., New York: McGraw-Hill, 1959, ch. 13, sec. 100, pp. 412-415.

Appendix A – MATLAB Code

```
%%%%%%%%%%%%%%%%%%%%%%%%%%%%%%%%%%%%%%%%%%%%%%%%%%%%%%%%%%%%%%%%%%%%%%%%%%%%%%%%
% SJA_Simulated_Frequency_Response                                              %
%                                                                               %
% This MATLAB script is used to simulate the frequency response of an           %
% SJA.                                                                          %
%                                                                               %
% Select an appropriate frequency range and set the design parameters.          %
%%%%%%%%%%%%%%%%%%%%%%%%%%%%%%%%%%%%%%%%%%%%%%%%%%%%%%%%%%%%%%%%%%%%%%%%%%%%%%%%

clear
clc
close all

%%%%%%%%%%%%%%%%%%%%%%%%%%%%%%%%%%%%%%%%%%%%%%%%%%%%%%%%%%%%%%%%%%%%%%%%%%%%%%%%
% Frequency Range

freq = linspace(0,8000,81);

%%%%%%%%%%%%%%%%%%%%%%%%%%%%%%%%%%%%%%%%%%%%%%%%%%%%%%%%%%%%%%%%%%%%%%%%%%%%%%%%
% Constants

a=347.22;                               % Speed of Sound in Air (m/s)
rho=1.1766;                             % Density of Air (kg/m^3)
mu=1.8714E-5;                           % Dynamic Viscosity of Air (N*s/m^2)
nu=mu/rho;                              % Kinematic Viscosity of Air (m^2/s)
dis=5e-6;                               % Diaphragm Displacement (m)

%%%%%%%%%%%%%%%%%%%%%%%%%%%%%%%%%%%%%%%%%%%%%%%%%%%%%%%%%%%%%%%%%%%%%%%%%%%%%%%%
% Design Parameters

Do=.84e-3;                              % Orifice Diameter
h=1.76e-3;                              % Orifice Height
H=.5e-3;                                % Chamber Height
Dc=12.28e-3;                            % Chamber Diameter
Vc=20e-9;                               % Chamber Volume

%%%%%%%%%%%%%%%%%%%%%%%%%%%%%%%%%%%%%%%%%%%%%%%%%%%%%%%%%%%%%%%%%%%%%%%%%%%%%%%%

Ao=pi*(Do/2)^2;                         % Area of orifice (m^2)

Cac=Vc/(rho*a^2);                       % Acoustic Capacitance of Chamber
Marad=16*rho/(3*pi^2*Do);               % Acoustic Radiation Mass
```

```
t_final = .1;                           % Simulation Stop Time
Qosim=0;

for i = 1:length(freq)
    omega = freq(i)*2*pi;               % Oscillation Frequency
    St=(omega*Do^2/nu)^5;               % Stokes Number
    A=pi^2/16*dis*freq(i)*Dc^2;

    K_r=Kr(St);                         % Correction Factors Found using
    K_m=Km(St);                         % Interpolation Functions
    K_anl=Kanl(St);

    Ral=K_r*128*mu*h/(pi*Do^4);         % Acoustic Linear Resistance and
    Mal=K_m*16*rho*h/(3*pi*Do^2);       % Linear Mass at Orifice
    Rarad=1/(2*pi)*rho*omega^2/a;       % Acoustic Radiation Resistance
    Ranl=K_anl*8*rho/(pi^2*Do^4);       % Nonlinear Resistance at Orifice

    for k=1:10;
        G=1/(Cac.*(Mal+Marad));         % Simulink Parameters
        G1=2*Cac*Ranl.*Qosim;      %

        sim('SJA_Block_Diagram',[0 t_final]);

        index = round(length(Qo(:,1))*4/5);
        Qo_ss = Qo(index:end,1);        % Steady State Current

%       Qosim = sqrt(mean(Qo_ss.^2));  % RMS Flow Rate
        Qosim = max(Qo_ss);             % Peak Flow Rate

    end

    v(i)=Qosim/Ao;

end

figure
plot(freq,v,'o','MarkerEdgeColor','k','MarkerFaceColor','b','MarkerSize',5)

%%%%%%%%%%%%%%%%%%%%%%%%%%%%%%%%%%%%%%%%%%%%%%%%%%%%%%%%%%%%%%%%%%%%%%%%%%%%%%%
% Figure Properties
xlabel('Frequency, Hz')
ylabel('Velocity, m/s')
```

Published with MATLAB® R2014a

```
function [ KmINT ] = Km( St )
%Km calculates the correction factor for the linear acoustic mass.
%   St - Stokes Number
%   KmINT - Correction Factor for the Linear Acoustic Mass

logSt=log10(St);

data= [ 0                   1
        0.492844412         0.998889199
        0.736714976           0.990882471
        0.914290629         0.964436006
        1.032674398           0.930710697
        1.243397507           0.867870014
        1.3854580293104348  0.8356004739939871
        1.558298331875934   0.8079408682708035
        1.716932582175776   0.7904716436035296
        1.8779345078532272  0.7778549813438318
        2.08865761646048    0.7671793440471645
        2.31358677733339    0.7601431285561792
        2.576398744         0.755533194
        2.853416763         0.752864285
        3                   0.751893772 ];


Xi=data(:,1)';
Yi=data(:,2)';

n=length(Xi);

a=zeros(n-1,1);
b=a;
c=a;
d=a;

f=cell(n-1,1);

dY=zeros(1,n-1);

for i=1:n-1
A=[  Xi(i)^2     Xi(i)     1
     Xi(i+1)^2   Xi(i+1)   1
   2*Xi(i)          1      0];

B=[Yi(i);Yi(i+1);dY(i)];

C=(A\B)';

dY(i+1)=2*C(1)*Xi(i+1)+C(2);


f{i}=@(X) C(1)*X.^2+C(2)*X+C(3);
end
```

```
KmINT=-1;

if logSt<=Xi(1)
    KmINT=1.00;
elseif logSt>=Xi(n)
    KmINT=0.75;
else
    for i=2:n
        if logSt<=Xi(i) && KmINT==-1
           KmINT=f{i-1}(logSt);
        end
    end
end
end
```

Published with MATLAB® R2014a

```
function [ KanlINT ] = Kanl( St )
%Kanl calculates the correction factor for the nonlinear acoustic mass.
%   St - Stokes Number
%   KanlINT - Correction Factor for the Nonlinear Acoustic Mass

logSt=log10(St);

data= [ 0,                      2
        0.22192513368983935,    1.9999999999999998
        0.5320788443272224,     1.9899511135252579
        0.6296629868677506,     1.9758283541553503
        0.7058507640871763,     1.952743074416078
        0.7633177882283226,     1.9234111895708852
        0.848831720728388,      1.852254209668658
        0.9603650654869622,   1.7061379684953828
        1.1132979634992604,     1.493753394894079
        1.2368739234373323,     1.3633894622487777
        1.2956636854534416,     1.3128734383487233
        1.3263972803085975,     1.29033134166214
        1.3651495423610165,     1.2637153720803909
        1.402566721469092,      1.2398153177620856
        1.4486724693333952,     1.2140141227593695
        1.496116749499662,      1.1906572514937532
        1.5582647334772137,     1.164041281912004
        1.6284346524645115,     1.1382400869092881
        1.6979392085212928,     1.1170559478544269
        1.7614309896098088,   1.1007604562737638
        1.8222506078131213,     1.0869092884302007
        1.8803984262215085,     1.0760456273764256
        1.9392154200083078,   1.0662683324280282
        1.9993700383713804,   1.057577403585008
        2.073561726799258,      1.048343291689299
        2.1450805261613803,   1.040467137425312
        2.2159319655964698,     1.0342205323193914
        2.290794644854139,      1.0287887017925037
        2.352957878623277,      1.0249864204236825
        2.4131159463439715,     1.0214557305812055
        2.4619109223364424,     1.0187398153177618
        2.5227381654355483,     1.0162954915806623
        2.5969343924918737,     1.0138511678435629
        2.6844997850505568,     1.0116784356328081
        2.7827601832298763,     1.0092341118957087
        2.8883737041308057,   1.0070613796849537
        3,      1.0057034220532317 ];

Xi=data(:,1)';
Yi=data(:,2)';

n=length(Xi);

a=zeros(n-1,1);
b=a;
c=a;
```

```
d=a;

f=cell(n-1,1);

dY=zeros(1,n-1);

for i=1:n-1
A=[  Xi(i)^2     Xi(i)     1
     Xi(i+1)^2   Xi(i+1)   1
   2*Xi(i)          1      0];

B=[Yi(i);Yi(i+1);dY(i)];

C=(A\B)';

dY(i+1)=2*C(1)*Xi(i+1)+C(2);


f{i}=@(X) C(1)*X.^2+C(2)*X+C(3);
end

KanlINT=-1;

if logSt<=Xi(1)
    KanlINT=2.00;
elseif logSt>=Xi(n)
    KanlINT=1.00;
else
    for i=2:n
        if logSt<=Xi(i) && KanlINT==-1
           KanlINT=f{i-1}(logSt);
        end
    end
end
end
```

Published with MATLAB® R2014a

```
function [ KrINT ] = Kr( St )
%Kr calculates the correction factor for the linear acoustic resistance.
%   St - Stokes Number
%   KanlINT - Correction Factor for the Nonlinear Acoustic Resistance

logSt=log10(St);

data=   [0         0
    0.0598    0.0023
    0.1266    0.0023
    0.3337         0
    0.4235         0
    0.5362    0.0023
    0.5961    0.0047
    0.6260    0.0070
    0.6513    0.0093
    0.6766    0.0117
    0.7181    0.0164
    0.7733    0.0257
    0.8308    0.0397
    0.8815    0.0584
    0.9413    0.0864
    0.9896    0.1145
    1.0380    0.1449
    1.0840    0.1776
    1.1530    0.2290
    1.2474    0.2991
    1.2750    0.3178
    1.3049    0.3388
    1.3993    0.4182
    1.4776    0.4860
    1.5627    0.5607
    1.6640    0.6519
    1.7745    0.7523
    1.8872    0.8575
    2.0138    0.9790];

Xi=data(:,1)';
Yi=data(:,2)';

n=length(Xi);

a=zeros(n-1,1);
b=a;
c=a;
d=a;

f=cell(n-1,1);

dY=zeros(1,n-1);

for i=1:n-1
A=[  Xi(i)^2     Xi(i)     1
```

```
     Xi(i+1)^2   Xi(i+1)   1
   2*Xi(i)          1      0];

B=[Yi(i);Yi(i+1);dY(i)];

C=(A\B)';

dY(i+1)=2*C(1)*Xi(i+1)+C(2);


f{i}=@(X) C(1)*X.^2+C(2)*X+C(3);
end

logKr=-1;

if logSt<=Xi(1)
    logKr=0;
elseif logSt>=Xi(n)
    logKr=logSt-Xi(n)+Yi(n);
else
    for i=2:n
        if logSt<=Xi(i) && logKr==-1
           logKr=f{i-1}(logSt);
        end
    end
end
KrINT=10^logKr;
end
```

Published with MATLAB® R2014a

```
%%%%%%%%%%%%%%%%%%%%%%%%%%%%%%%%%%%%%%%%%%%%%%%%%%%%%%%%%%%%%%%%%%%%%%%%%%%%
% SJA_Experimental_Frequency_Response                                        %
%                                                                           %
% This MATLAB script processes CTA data to plot the RMS and peak velocity %
% frequency responses from SJA experiments.                                 %
%                                                                           %
% Run this script in the same folder as the CTA data.                       %
%%%%%%%%%%%%%%%%%%%%%%%%%%%%%%%%%%%%%%%%%%%%%%%%%%%%%%%%%%%%%%%%%%%%%%%%%%%%

clear
clc
close all

%%%%%%%%%%%%%%%%%%%%%%%%%%%%%%%%%%%%%%%%%%%%%%%%%%%%%%%%%%%%%%%%%%%%%%%%%%%%
% Frequency Range

freq=0:100:8000;

%%%%%%%%%%%%%%%%%%%%%%%%%%%%%%%%%%%%%%%%%%%%%%%%%%%%%%%%%%%%%%%%%%%%%%%%%%%%
% Post Processing

vmax=zeros(1,81); % Initialization of Peak Velocity Vector
vrms=zeros(1,81); % Initialization of RMS Velocity Vector

for i=1:81                                      % A data file containing
data = csvread(strcat('CTA_Data_',...           % time response data is
    int2str((i-1)),'.csv'),2);                  % read at each frequency.

t=data(:,1);                                    % Time Data
V=data(:,2);                                    % Voltage Data

Vmax=max(V);                                    % Maximum Voltage

vmax(i)=8.8516.*Vmax.^4-49.4981.*Vmax.^3+...    % Peak Velocity
    118.1419.*Vmax.^2-136.8463.*Vmax+61.6152;

v=8.8516.*V.^4-49.4981.*V.^3+118.1419.*...      % Velocity Data
    V.^2-136.8463.*V+61.6152;
vrms(i)=sqrt(mean(v.^2));                       % RMS Velocity
end

%%%%%%%%%%%%%%%%%%%%%%%%%%%%%%%%%%%%%%%%%%%%%%%%%%%%%%%%%%%%%%%%%%%%%%%%%%%%
% Plotting

figure
plot(freq,vmax,'o','MarkerEdgeColor','k',...
    'MarkerFaceColor','b','MarkerSize', 5)

xlabel('Frequency, Hz')
ylabel('Velocity, m/s')

figure
plot(freq,vrms,'o','MarkerEdgeColor','k',...
```

```
    'MarkerFaceColor','b','MarkerSize', 5)

xlabel('Frequency, Hz')
ylabel('Velocity, m/s')
```

Published with MATLAB® R2014a

Appendix B – CTA Calibration

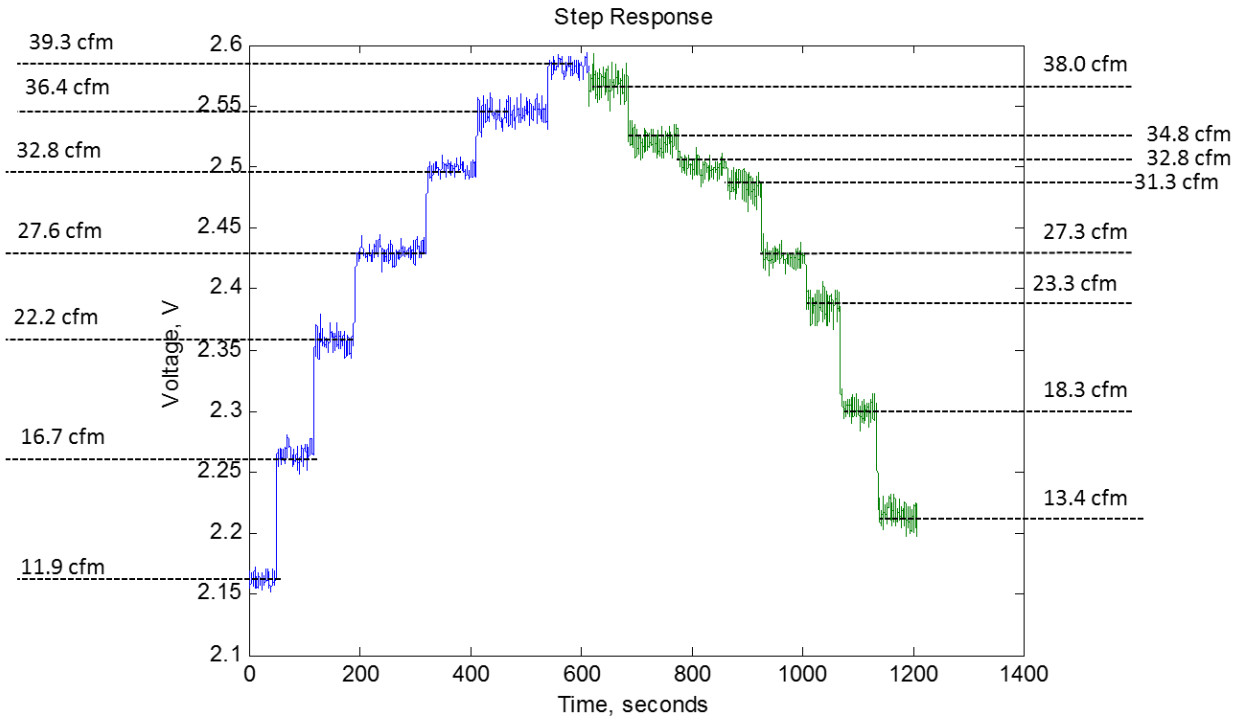

Step Up Points

Flow (cfm)	Velocity (m/s)	Average Voltage
11.9	11.08	2.162
16.7	15.55	2.264
22.2	20.67	2.357
27.6	25.70	2.430
32.8	30.55	2.499
36.4	33.90	2.545
39.3	36.60	2.583

Step Down Points

Flow (cfm)	Velocity (m/s)	Average Voltage
38.0	35.39	2.567
34.8	32.41	2.520
32.8	30.55	2.499
31.3	29.15	2.485
27.3	25.42	2.426
23.3	21.70	2.387
18.3	17.04	2.302
13.4	12.48	2.215

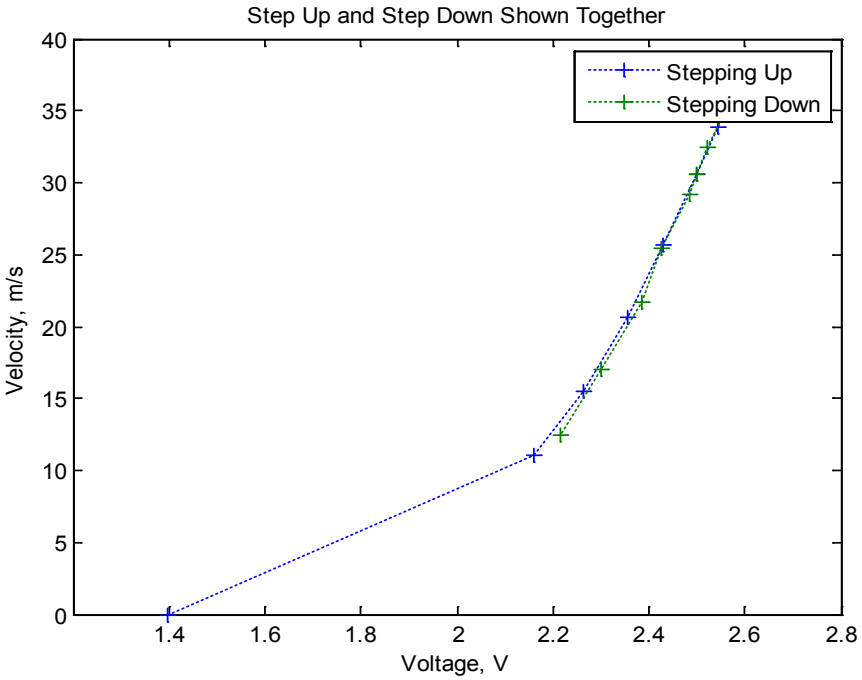

Plot Showing Mirrored Velocities

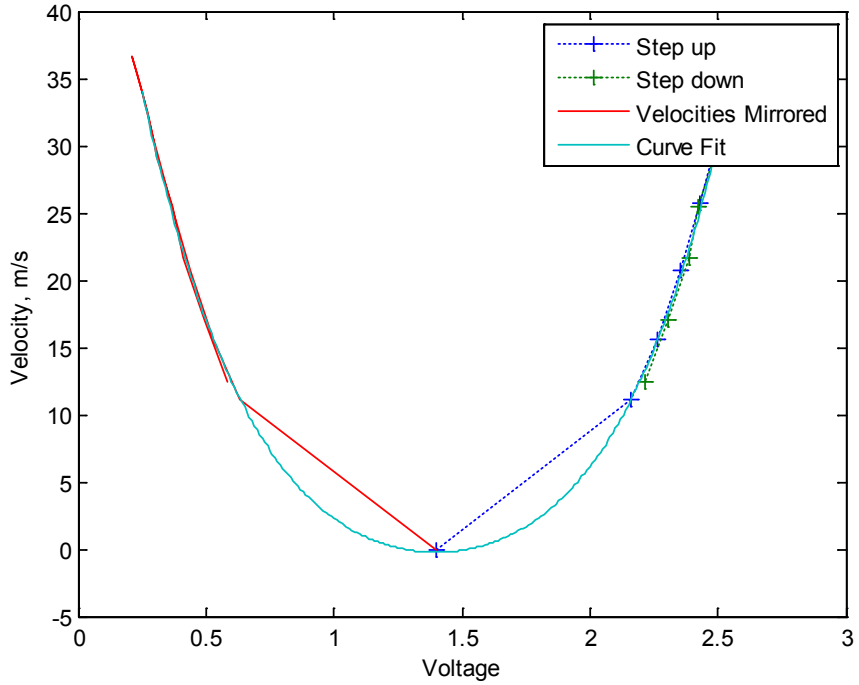

Plot Showing Resultant Curve Fit

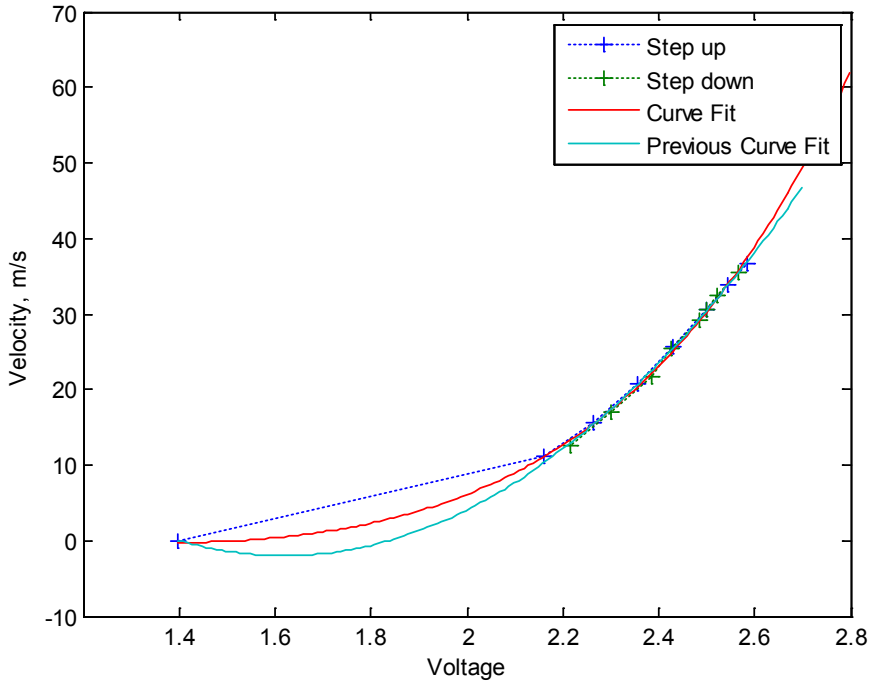

Fourth Order Curve Fit:

$$\text{Velocity} = 8.8516\,E^{4} - 49.4981\,E^{3} + 118.1419\,E^{2} - 136.8463\,E + 61.6152$$

Appendix C – Technical Drawings

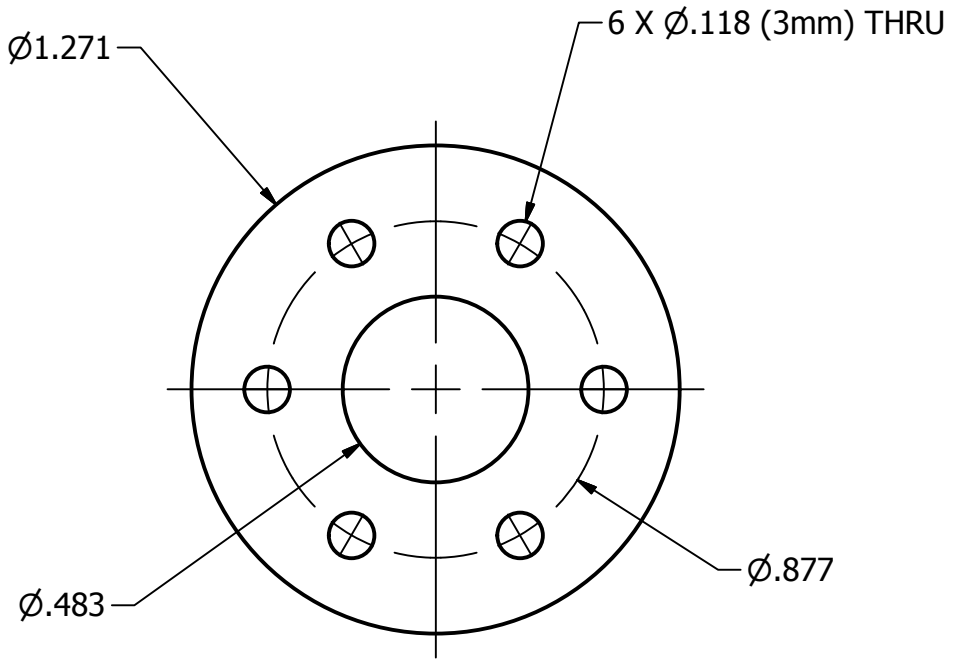

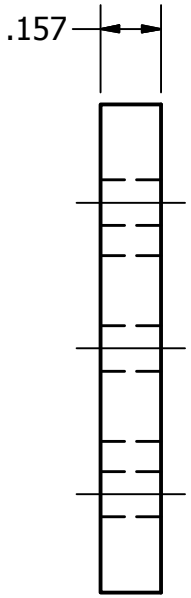

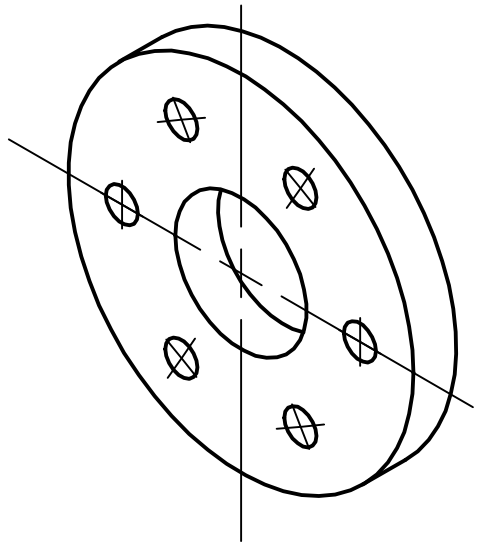

DRAWN thornton.254	4/13/2015	All units are in inches unless otherwise specified.
CHECKED		TITLE: SJA Cover for Array
QA		
MFG		
APPROVED		
		SIZE A | DWG NO 1 | REV
		SCALE 2:1 | SHEET 1 OF 1

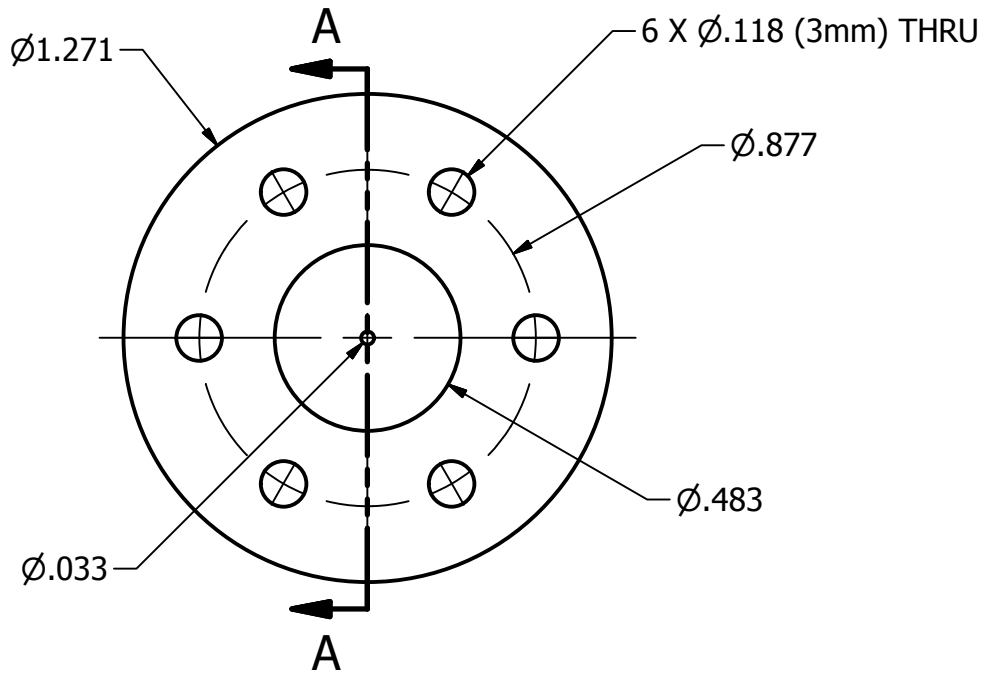

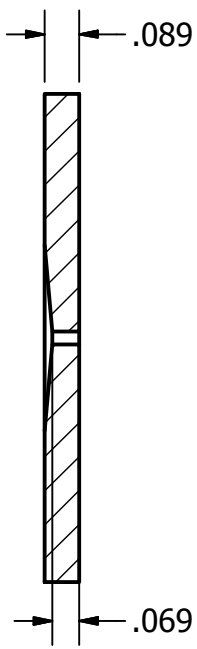

SECTION A-A

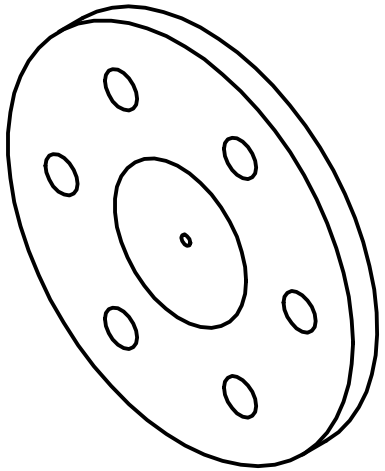

DRAWN thornton.254	4/13/2015	All units are in inches unless otherwise specified.	
CHECKED		TITLE	
QA		SJA for Array	
MFG			
APPROVED			
		SIZE A	DWG NO 2 / REV
		SCALE 2:1	SHEET 1 OF 1